This article has been accepted for publication in IEEE Internet of Things Journal. This is the author's version which has not been fully edited and content may change prior to final publication. Citation information: DOI 10.1109/JIOT.2024.3355702

Power-adaptive Communication with Channel-aware Transmission Scheduling in WBANs

Abbas Arghavani, Haibo Zhang, Zhiyi Huang, Yawen Chen,

***Abstract*—Radio links in Wireless Body Area Networks (WBANs) are highly subject to short and long-term attenuation due to the unstable network topology and frequent body blockage. This instability makes it challenging to achieve reliable and energy-efficient communication, but on the other hand, provides a great potential for the sending nodes to dynamically schedule the transmissions at the time with the best-expected channel quality. Motivated by this, we propose IGE (Improved Gilbert-Elliott Markov chain model), a memory-efficient Markov chain model to monitor channel fluctuations and provide a long-term channel prediction. We then design ATPS (Adaptive Transmission Power Selection), a deadline-constrained channel scheduling scheme that enables a sending node to buffer the packets when the channel is bad and schedule them to be transmitted when the channel is expected to be good within a deadline. ATPS can self-learn the pattern of channel changes without imposing a significant computation or memory overhead on the sending node. We evaluate the performance of ATPS through experiments using TelosB motes under different scenarios with different body postures and packet rates. We further compare ATPS with several state-of-the-art schemes including the optimal scheduling policy in which the optimal transmission time for each packet is calculated based on the collected RSSI (Received Signal Strength Indicator) samples in an off-line manner. The experimental results reveal that ATPS performs almost as efficiently as the optimal scheme in high-date-rate scenarios and has a similar trend on power level usage.**

***Index Terms*—WBAN, Sensor Networks, Channel Prediction, Markov Chain, Energy-aware, Power-adaptive Communication.**

I. Introduction

OWING to technological advancements in designing tiny communication and computing hardware, the idea of using wearable sensors to monitor human health has attracted tremendous interest. Motivated by this, the so-called Wireless Body Area Networks (WBAN), a particular type of Wireless Sensor Network (WSN) composed of a group of in-body and/or on-body tiny sensors, has been standardized in IEEE 802.15.4 [1] and IEEE 802.15.6 [2] for the MAC and PHY layers. In addition to health monitoring [3], WBANs support a vast variety of applications from gaming and entertainment [4], to fitness and sport [5], assisting with visual or aural disabilities [6], and safety applications [7].

Due to the ever-increasing trend of miniaturizing sensors' components, particularly the battery, *energy efficient* communication for WBANs to guarantee the long-lasting operation of body sensors appears to be imperative, though challenging. This is more problematic when it comes to the implanted sensors, which are expected to operate for several years. On the other hand, WBANs drastically suffer from unstable channel quality due to the frequent movements of the body or body parts. Considering the inevitable demand for *reliable* delivery of body sensor's crucial measurements, designing an ultra-reliable communication protocol over the unstable WBAN's channels is impossible to diminish. These concerns become more challenging when high transmission power should be used as little as possible to reduce *interference*. According to the IEEE 802.15 working group document, the transmission range of WBANs is expected to be less than 3 meters when there could be up to 10 WBANs in a space of $6m^3$ [8].

A. Motivation & Challenges

This research primarily addresses the challenges in developing a power-adaptive communication protocol for WBANs. This need arises from the dynamic topology of WBANs, exemplified in Fig. 1, which shows different postures in a walking gait cycle and their impact on the WBAN's topology. Our previous work, Chimp [9], demonstrated the initial exploration of adapting transmit power in response to body motion and channel fluctuations. Chimp's approach, which utilized angular velocity data in a reinforcement learning algorithm, highlighted the potential for power adjustment based on channel conditions. However, it exhibited limitations in terms of slow adaptation to significant posture changes and lacked long-term channel prediction and scheduling mechanisms. This highlighted a gap in achieving efficient low-power

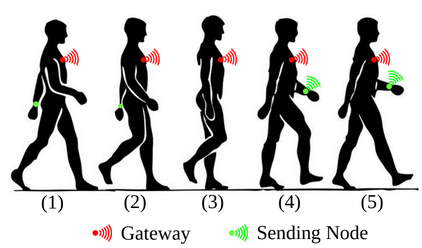

Figure 1: Topology instability in WBANs [9].

TABLE I: PDR of Power Levels in Different Postures [9].

P:power level; T:transmission range (m); e:current usage (mA)

P	T	e	Packet Delivery Rate (PDR)				
			(1)	(2)	(3)	(4)	(5)
1	1.2	7.6	0%	0%	0%	63.6%	84.3%
2	1.5	8.1	0%	7.1%	17.3%	88.3%	96.1%
3	35.5	8.5	92%	96.8%	95%	99.5%	99.3%
4	40.5	8.85	96.3%	99.2%	97.4%	≈100%	≈100%
5	44.5	9.2	96.6%	99.4%	97.4%	≈100%	≈100%
6	50.2	9.55	96.7%	99.4%	97.4%	≈100%	≈100%
7	> 50	9.9	99.2%	99.4%	98.7%	≈100%	≈100%

A. Arghavani is with the Embedded System Division, IDT Department, Mälardalens University, email: abbas.arghavani@mdu.se; and H. Zhang, Z. Huang, and Y. Chen are with the Department of Computer Science, University of Otago, emails: {haibo, hzy, yawen}@cs.otago.ac.nz.

communication, particularly when a Line-of-Sight (LoS) path is anticipated to be available.

Table I shows the measurements for the seven lowest power settings of the CC2420 radio [10] on the TelosB sensor platform [11]. The data indicates that higher power levels, while ensuring a better Packet Delivery Rate (PDR), also result in increased energy consumption and a broader interference range. Conversely, lower power levels are more energy-efficient but show reduced PDR, especially in the absence of a LoS path. These observations underline the need for a more nuanced approach to power management in WBANs, one that can dynamically adapt to changing channel conditions and posture-related obstructions. This paper thus focuses on three primary research challenges:

(1) Developing a method for a sending node in a WBAN to predict highly unstable channel quality over extended periods, despite rapid changes in body posture.
(2) Determining how a sending node can select the most appropriate transmission power level based on this predicted channel quality, striking a balance between energy efficiency and communication reliability.
(3) Designing a scheduling mechanism that allows the sending node to choose its optimal transmission time, taking advantage of periods with favorable channel conditions.

By addressing these challenges, we aim to enhance the adaptability and efficiency of communication protocols in WBANs, building on the insights gained from our previous research and extending them with advanced prediction and scheduling capabilities.

B. Novelty & Contributions

This paper introduces a novel communication method, Adaptive Transmission Power Selection (ATPS) for WBANs. The **key idea** of ATPS is to provide a long-term channel prediction for the sending node to maximize its performance through jointly adjusting the transmission power level and rescheduling the packet if the channel quality is expected to be better within the packet deadline. In this paper, a new memory-efficient Markov chain model is designed to address Challenge (1) by utilizing the relatively large channel coherence time in WBANs (up to 70 ms [12]) and the periodic nature of body activities (e.g., walking, jogging, running, and cycling). Challenge (2) is addressed by utilizing a cost function proposed in [9], through which the transmission cost of each power level at a given channel quality can be estimated. Finally, challenge (3) is addressed by introducing an optimal deadline-constrained scheduling policy, using which the sending node can select the best transmission time based on the long-term channel prediction. Overall, each sending node in ATPS can self-estimate its channel behavior and dynamically adjust its transmission power or schedule to achieve high communication reliability, low energy consumption, and low interference. The major contributions of this work are summarized as follows:

- We present a comprehensive analysis of channel behavior study using two established models, leading to the following key findings: (1) The Gilbert-Elliott (GE) Markov chain model, while widely used, does not offer the precision necessary for accurately capturing channel behavior in WBANs. (2) The Extended GE (EGE) model, though achieving high prediction accuracy, incurs substantial memory complexity, which limits its suitability for resource-constrained body sensors. Building on this analysis, we introduce the Improved GE Markov chain model (IGE). IGE retains the predictive accuracy benefits of the EGE model and effectively mitigates its memory complexity issues. This approach allows for a detailed comparative analysis of these three channel prediction models.
- ATPS is designed to dynamically adjust the transmission power at a per-transmission level using a channel prediction model.
- A channel-aware deadline-constrained scheme for scheduling packet transmissions is proposed to improve the performance of ATPS. Based on the designed IGE model, each sending node makes decisions on packet transmissions to minimize the transmission cost, i.e., to transmit immediately or wait for a future time frame with better channel quality.
- The performance of the proposed channel model and communication protocol is evaluated through experiments on the TelosB sensor motes under different packet rates and body postures. The results reveal a significant reduction in energy consumption and interference range.

The remainder of this paper is structured as follows: Section II provides an overview of related works. Section III analyzes channel behavior. Section IV explores two established models for predicting channel behavior, and introduces the innovative IGE model. Section V introduces ATPS and discusses the optimal deadline-constrained transmission scheduling policy. Section VI evaluates the proposed channel model and communication protocol. Section VII concludes this paper and outlines potential future works.

II. Related Works

A. Channel prediction models

Pilot-based techniques have been widely used for estimating the communication channel characteristics between the sending node and the gateway [13], [14]. In [13], where the focus of the paper is on exploring the potential utilization of optical wireless channels in WBANs, both the sending node and the gateway periodically exchange pilot symbols. This facilitates channel estimation at the gateway to obtain channel characteristics accurately for the sensor-gateway link. Notably, an optimal pilot-based channel estimation technique is proposed in [14] specifically for EEG signal transmission, aiming to mitigate channel-induced decoding errors at the receiver. However, it is important to acknowledge that pilot symbols necessitate the allocation of a dedicated portion of the available bandwidth or time resources for transmission, which might be less desirable in WBANs characterized by highly time-varying channels.

According to [12], a practical channel estimator for WBANs should be able to quickly adapt its estimations with sharp channel fluctuations and should be lightweight so that the resource-constrained sending nodes can perform it and estimate the channel in a real-time manner. Lightweight linear estimators such as linear least squares have been widely used to estimate the channel quality in wireless networks [15], [16]. However, they cannot predict the rapid channel dynamics in WBANs because (1) they essentially behave like a filter that generates a delayed version of the channel waveform [17], and (2) they assume a linear relationship between the transmission signal power and the Received Signal Strength Indicator (RSSI). DPPI [18] avoids delay in channel prediction by utilizing a built-in linear model. In DPPI, the gateway compares the RSSI of the latest received packet with a predefined optimal RSSI range ($[RT_L, RT_H]$). If the measured RSSI falls in the optimal range, the used transmission power is considered to be optimal; otherwise, the optimal transmission power level is calculated using the linear model and reported to the sending node. In the same way, RL-TPC [19] uses a built-in linear model. However, it first measures the Link Quality Indication (LQI) of the received packet to make sure the received RSSI is not increased by an interferer. If the LQI is low, RL-TPC switches its channel frequency to avoid interference. Although DPPI and RL-TPC can avoid delay in prediction, they cannot model instant channel fluctuations. Besides that, due to the rapid channel fluctuations in dynamic body postures, the assumption of a linear relationship between transmission power and RSSI degrades their performance. Moreover, by considering only the RSSI of the last received packet, DPPI and RL-TPC may encounter the ping-pong effect in which the sending node iteratively alternates between two adjacent power levels i and $i+1$ because the RSSI of power level i is less than RT_L and the RSSI of power level $i+1$ is higher than RT_H [9].

To compensate for the drawbacks of the above methods while keeping their advantages (e.g., low complexity), a linear prediction-based power-adaptive communication protocol for WBAN is proposed in [17]. It combines the ability of finite-state Markov chain models to describe the behavior of a complex system with the simplicity of linear estimators. This method benefits from the reciprocity of WBAN wireless channels [20] and assumes the on-body channels are relatively stable for a short period and the channel prediction is valid for up to 1 second. Similarly, a lightweight linear channel prediction algorithm is presented in [21] to enable a sending node to track the channel quality variation. It combines linear channel prediction with the Finite State Markov Chain (FSMC) model so that a sending node can monitor the channel history and extract the channel properties (i.e., the statistics of the channel behavior). In this model, the states in the Markov chain represent the RSSI sub-ranges and the transition probabilities between different states are maintained using a large-size Transition Matrix (TM). Although this method has a very low computational complexity, its memory complexity is extremely large in the order of $O(M^{L+1})$, where M is the number of RSSI sub-ranges and L is the length of history of the latest channel observations. Moreover, it only predicts the next channel state upon receiving a packet, and thereby cannot be used for transmission scheduling to save energy and reduce interference in delay-tolerant applications.

The GE model [22], [23] has been extensively used to predict the behavior of a network link with a special focus on burst error patterns. In [24] a centralized communication protocol based on the GE model is proposed to provide a reliable and energy-efficient TDMA-based communication. In this method, the gateway estimates the channel fluctuations of the wireless links and adjusts the transmission schedule to minimize the energy consumption subject to desirable network communication reliability and throughput constraints. This method assumes that some channel parameters such as the transition probability between different channel states are constant as long as the body posture does not change. However, in the GE model, the next state of the channel depends only on the current state and the transit probabilities, and not on the channel history. Hence, it cannot achieve high accuracy in long-term channel prediction. The Extended Gilbert-Elliott model (EGE) [25] extends the GE model to remember the channel history by introducing internal sub-states. The accuracy of EGE depends on the number of internal sub-states. Its major drawback is the high memory complexity.

B. Power-adaptive communication

ExPerio [26], LPA [27], G-TPC [28], and M-TPC [29] utilize the correlation between body motion pattern and channel fluctuation. In these schemes, the sending node continuously monitors the local acceleration signal to find a periodic motion. Once the periodicity is detected, it measures the RSSI of the received packets to find the RSSI peaks. By comparing the acceleration peaks and RSSI peaks over the same period (e.g. 10 seconds), the sending node can approximate the time offset between an acceleration peak and its corresponding RSSI peak. Then, the transmissions are scheduled at the channel peaks to achieve a high PDR using a low transmission power level. However, these schemes suffer from high computation overhead. For example, ExPerio has to perform about 100000 arithmetic operations to learn channel periodicity [26].

Chimp [9] also utilizes the correlation between body motion pattern and channel fluctuation, but has low computation complexity. Chimp feeds the locally measured angular velocity data into a lightweight reinforcement learning algorithm. In combination with the received ACK packets, it gradually learns the optimal power level under each sub-range of angular velocity. Although Chimp is lightweight, simple, and finds the optimal transmit power level for a given channel quality, its learning process is quite slow when the body posture is changing (e.g., from standing to running). This problem is avoided in Tuatara [30] by roughly estimating the real-time location of the sending node relative to the gateway. Due to the strong correlation between the location of a sending node relative to the gateway and the channel quality, the sending node can quickly adjust its power level before transmission, when its current location is known. Although both Chimp and particularly Tuatara achieve near-optimal results, they transmit the packets as soon as they are generated without exploring the advantage of dynamic transmission scheduling to further reduce energy consumption and interference.

C. Dynamic transmission scheduling

Transmission scheduling in WBANs has been investigated generally from two different perspectives: (1) focusing on reducing energy usage (e.g., ExPerio [26]); and (2) focusing on prioritizing the emergency packets (e.g., EEEA-MAC [31]). EEEA-MAC is an emergency-first slot allocation scheme for multip-hop WBANs, in which the emergency data is handled by relay nodes according to different criteria. Besides, several papers have investigated transmission scheduling for general WSNs. Soldati *et al*. [32] developed a mathematical programming framework for joint routing and link scheduling of deadline-constrained traffic in wireless sensor networks with linear network topology. In [33], a reliable, energy-efficient, and deadline-constrained routing protocol is proposed for multi-hop communication networks. In this paper, the lossy channel is modeled using a simple Markov chain model. It is shown that the probability that a packet is delivered within a deadline is maximized under the proposed policy. It is also shown that an increasing number of paths between source and destination achieve high reliability when links become more bursty. In [34] a two-stage transmission scheduling policy for real-time heterogeneous periodic traffic in one-hop WSNs was investigated. However, all the above schemes assume both network topology and sensor positions are constant. Therefore, these existing schemes do not apply to WBANs.

Unlike most of the aforementioned schemes, our scheme ATPS is self-organized and needs neither information about the current body posture nor the location of the sending node. It can self-estimate the channel quality in both static and dynamic postures even when the motion patterns (and consequently the channel properties) of the subject are changed during a single posture (e.g., when the subject increases or decreases walking speed). The proposed model is highly memory efficient and lightweight. Hence, it can be used by the sending node for power-adaptive communication without imposing a problematic overhead. It can provide a long-term channel prediction that makes the use of scheduling policies beneficial for delay-tolerant applications.

III. Channel Characterising

The variation in WBAN's channel quality can be characterized using the RSSI, as detailed in [18] and [30]. Additionally, dividing the RSSI range into several coarse-grained sub-ranges through RSSI thresholding is a practical and commonly used method to classify channel quality into distinct states [35]. Assuming that the channels in WBANs are symmetric, there are two methods for informing the sending node about channel quality, based on RSSI measurements: (1) The gateway measures the RSSI of incoming packets and includes this data in ACK packets. While feasible, this method is complex due to varying transmission power levels of the sending node, complicating the interpretation of RSSI values. (2) The sending node measures the RSSI of ACK or beacon packets from the gateway. As the gateway, often a mobile phone, doesn't have battery constraints and can maintain stable transmission power, this method is simpler and more reliable, avoiding the need to account for variable power levels. We chose the second approach for its simplicity and elimination of the need for extra data in ACK packets.

Guided by this assumption, this section begins with an investigation into channel symmetry within WBANs. Following this, we proceed to delineate the channel's behavior during daily physical activities. Our investigations indicate that channels in WBANs exhibit a significant degree of spatio-temporal locality. That is, the channel tends to remain in the same state for a long period before transitioning to a different state. This characteristic can be leveraged to enhance channel prediction and scheduling effectiveness. Ultimately, we elucidate the process of mapping channel quality onto channel states (represented by RSSI sub-ranges) using RSSI thresholding. To this end, we carry out experiments to collect RSSI samples across different static and dynamic postures including standing, sitting, driving, walking, and running. In these experiments, the same one-hop star topology as presented in Fig. 1 is adapted with the sending node attached to the wrist and the gateway mounted on the chest.

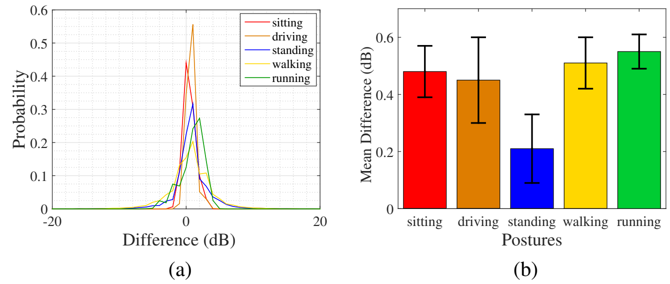

Figure 2: (a) Probability distribution of difference of RSSI at sending node and gateway (b) Mean and standard deviation of the differences.

A. Validation on Channel Symmetry

To justify the symmetry of wireless channels in WBANs, the gateway and the sending node periodically exchange packets. For each packet received from the gateway, the sending node measures the RSSI and promptly responds by incorporating the measured RSSI value into its reply packet. Conversely, the gateway measures the RSSI for each packet received from the sending node, allowing it to determine the RSSI for the link in both directions. Fig. 2(a) shows the probability distribution of the difference between the measured RSSIs at the sending node and the gateway for power level 7. According to the three-sigma-rule of thumb (also called the 68–95–99.7 rule), if at least 65%, 95%, and 99.7% of the samples lie in the first, second, and third standard deviations of the sample set, respectively, the distribution is normal with high certainty. By analyzing the difference in RSSIs from and to the gateway, we observe that their distribution follows the three-sigma rule of thumb and thus it has a normal distribution in all postures. The mean and the standard deviation of differences in RSSIs between measured samples are depicted in Fig. 2(b). With mean and standard deviation values below 1 dB for each distribution, it can be inferred that the channel is symmetric at power level 7. This observation holds for experiments conducted at other power levels as well.

B. Channel behaviour analysis

Power adaptive communication is possible if the sending node adjusts its transmission power to a low power when the

This article has been accepted for publication in IEEE Internet of Things Journal. This is the author's version which has not been fully edited and content may change prior to final publication. Citation information: DOI 10.1109/JIOT.2024.3355702

LoS path to the gateway is available and switches to a high power when the LoS path is blocked. However, due to the topology instability, the LoS path is frequently disconnected. To enhance analytical clarity, we have simplified our model of channel behavior to encompass two distinct states, denoted as $\Omega = \{G, B\}$. Here, Ω represents the set of channel states. The state 'G' signifies the presence of the LoS path, indicative of a favorable channel condition, while 'B' indicates its absence, corresponding to an unfavorable channel state.

To analyze the channel's behavior, specifically the pattern of LoS path availability, we conducted a series of measurement campaigns. In our setup, time is divided into frames, and the beginning of each frame is indicated by a beacon packet transmitted by the gateway [1], [2]. The gateway adjusts its power level to level 1 due to the higher sensitivity of lower power levels to body blockage. Following the channel symmetry in WBANs, the sending node can classify the channel state based on the reception of the beacon packets. That is if the beacon packet is received, the channel is classified as being in the G state; otherwise, it is classified as being in the B state. The sequence of channel states observed over time is considered as a discrete-time time series $X = \{x_t\}_{t=1}^{N}$ where N is the total number of frames (i.e., the total number of observations) and t is the frame number, so x_t is the t^{th} observation. We introduce the term "state-duration," which quantifies the duration for which the channel remains in a particular state (state 'i') before transiting to a different state. The observations are grouped in the form of *i-state-duration* $\{i_r^c\}_{r=1}^{n}$, where i_r^c represents the r^{th} time that state $i \in \Omega = \{G, B\}$ is observed for exactly c ($c \in \{1, 2, 3, \ldots, N\}$) consecutive times. For example, the observation set $\{GGBBGGBBBGGGBBBBBGGGBB\ldots\}$ can be represented by $\{G_1^2, B_1^2, G_2^2, B_1^3, G_1^3, B_1^5, G_2^3, B_2^2, \ldots\}$. This representation of channel state observations helps illustrate the high-level overview of channel behavior, specifically, the transitions between channel states.

Fig. 3 shows the distribution of the length of state-durations (i.e., length of being in state G or B) during 5 minutes of walking and running. By analyzing the state-durations, we observe that the distribution of the length being in a state follows the three-sigma rule of thumb and thus it has a normal distribution. Following this observation and to analyze the

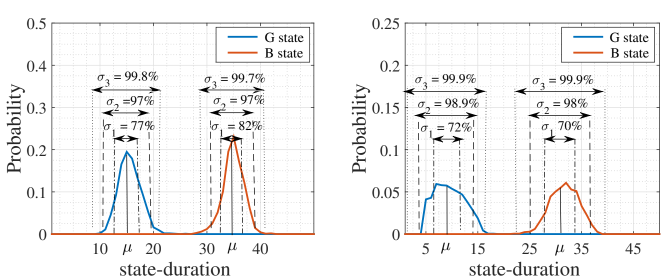

(a) (b)

Figure 3: Distribution of state-durations: (a) walking, (b) running.

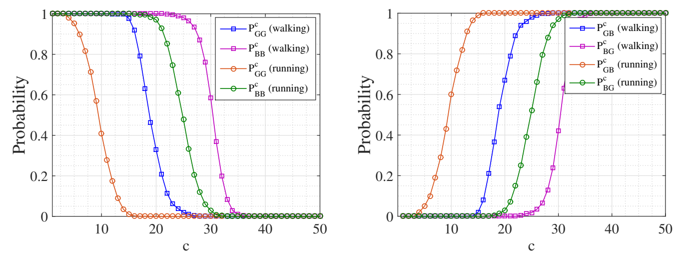

(a) (b)

Figure 4: (a) P_{ij}^c for $j = i$ and (b) P_{ij}^c for $j \neq i$ during walking and running.

long-term channel state transition more accurately, we propose the following metric:

- $P_{ij}^c(t)$: assuming the channel moves to state i at frame t, $P_{ij}^c(t)$ is defined as the probability of observing $c-1$ consecutive channel states in the current state i after t and observing the state j at frame $t+c$, that is,

$$P_{ij}^c(t) = P\big(x_{t+1} = x_{t+2} = \cdots = x_{t+c-1} = i, \wedge \\ x_{t+c} = j \mid x_t = i \wedge x_{t-1} \neq i\big) \tag{1}$$

where $i, j \in \Omega$ and c stands for *consecutive*. We plot it for different states using the collected channel observations to show how $P_{ij}^c(t)$ can characterize channel behavior. For scenarios with static body postures such as standing and sitting, it is observed that the channel quality remains stable, that is, $P_{GG}^c(t)$ is close to 1 when the LoS path is available, and $P_{BB}^c(t)$ is close to 1 when the LoS path is blocked by the human body. However, the channel quality during dynamic postures is quite unstable. Fig. 4 shows $P_{ij}^c(t)$ during walking and running. As can be seen from Fig. 4, $P_{ij}^c(t)$ for the case $j \neq i$ (Fig. 4(b)) has the reverse trend to that $P_{ij}^c(t)$ with $j = i$ (Fig. 4(a)), however, this is the case only for Markov models with two states. $P_{ij}^c(t)$ looks like an *S-shaped* logistic function, which indicates the existence of spatio-temporal locality among RSSI samples. That is, if the channel moves to state i, the probability the channel moves to another state j is low at the beginning but will gradually increase. If each sending node knows $P_{ij}^c(t)$, it can predict the long-term channel state transitions and adjust its transmission power to save energy and reduce interference. To acquire this information (i.e., $P_{ij}^c(t)$), Section IV initially scrutinizes two established channel models. Subsequently, it introduces the proposed channel model, designed to provide precise estimations of $P_{ij}^c(t)$. Before this, we elucidate the process by which channel quality is translated into multiple channel states through RSSI thresholding.

C. Classifying channel quality into multiple states

In our previous discussion, we classified channel quality into two states: Good (G) and Bad (B). Moving forward, we will outline a method for dividing channel quality into several states. For this purpose, we partition the RSSI range of the CC2420 radio chip, which spans from -90dBm to 0dBm, into multiple sub-ranges. Each of these sub-ranges is termed as a state i. In each state i, we configure a corresponding power

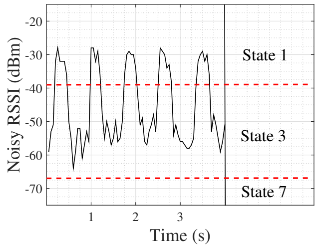

(a) Noisy RSSI

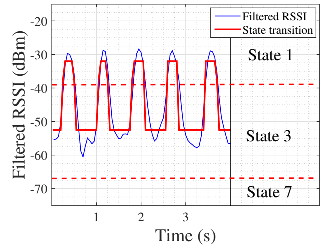

(b) Filtered RSSI

Figure 5: Partitioning RSSI range into a few channel states

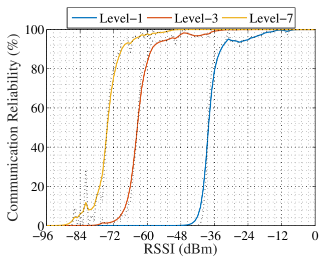

(a)

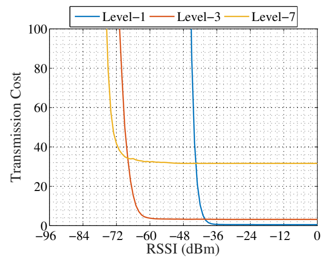

(b)

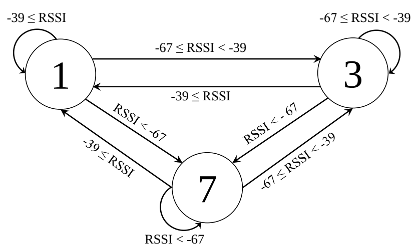

(c)

Figure 6: (a) Reliability of different power levels under different channel quality, (b) transmission cost of different power levels under different channel quality, and (c) state transition according to the RSSI range.

level, also labeled as i, to minimize transmission costs. We will later explain this concept of reducing transmission costs in more detail.

As discussed in Section I (also in [9]), power levels 1, 3, and 7 of the CC2420 radio chip are enough to provide short-range reliable communications in WBANs. Therefore, the channel quality can be classified into three states ($\Omega = \{1, 3, 7\}$). Fig. 5(a) shows the RSSI variation during running. Following what was said, the RSSI range is partitioned into 3 sub-ranges, each of which represents a channel state. Someone may argue that since the RSSI is noisy, its irregular fluctuations may influence the channel state transition pattern. Due to the limited RSSI fluctuation, a coarse-grain classification of RSSI range into a few channel states limits the effects of noise, as demonstrated in Fig. 5(b) which shows filtered RSSI (smoothed using a simple weighted averaging filter) and state transition of the same period during running.

To find the boundaries of the corresponding RSSI range per each channel state i, three rounds (called round-1, round-3, and round-7) of experiments in different postures have been carried out. In round i, the sending node periodically transmits a packet using power level i. Given that the sending node and the gateway are synchronized, the gateway sends back an ACK or NACK packet with power level 7 depending on the delivery status of the packet transmitted by the sending node. When the sending node receives the ACK/NACK, its RSSI is measured. By counting the number of ACK packets, the communication reliability with power level i per each sub-range of RSSI can be calculated. Fig. 6(a) shows the communication reliability of different power levels. As is expected, the communication reliability of all power levels is increased as the RSSI increases. By knowing the communication reliability of each power level i at each state, the transmission cost of the power level is calculated according to the following cost function introduced in [9]:

$$cost_i = \frac{P_{tx}^i}{r_i} \tag{2}$$

where P_{tx}^i is the transmission signal power of power level i and r_i is its corresponding reliability. Fig. 6(b) shows how the transmission cost of different power levels is changed with the increase in RSSI (i.e., with the increase in reliability). By comparing the transmission cost of each power level, the RSSI boundaries for each state i are defined as follows: the RSSI boundaries for state i are a range of RSSIs within which the transmission cost using power level i is lower than that of other power levels. For example, as can be seen in Fig. 6(b), the transmission cost of power level 3 in the RSSI range of -67 dBm to -39 dBm is lower than the transmission cost of other power levels. Fig. 6(c) shows the state transition machine with RSSI boundaries (i.e., the optimal RSSI range), where each link is labeled with the channel state transition criteria. Hence, a transition from any state to state i occurs if the measured RSSI falls in the RSSI boundaries of state i.

IV. Channel Modeling

In this section, we first describe two well-established Markov models for channel prediction. Following this, our proposed model is introduced and examined in detail. The third subsection provides an extensive analysis of each model, highlighting its strengths and weaknesses. We also present experimental results using collected channel data to demonstrate the superior performance of our proposed model. To simplify our explanation, we assume the channel alternates between two states: G and B.

A. Gilbert-Elliott (GE) Model and Its Extended Version

The GE model has been widely used to model burst error patterns of communication links. As illustrated in Fig. 7, it is a simple Markov chain with two states G and B. The link transits between two states with probability P_{GB} from G to B and P_{BG} from B to G, and remains in G state with probability P_{GG} and in B state with probability P_{BB}. These probabilities are commonly represented using the Transition Matrix (TM). Based on the collected channel observations, the TMs for walking and running are calculated, as shown in Fig. 7. It can be seen that, for both walking and running, P_{BB} and P_{GG} are close to 1, indicating the existence of high state

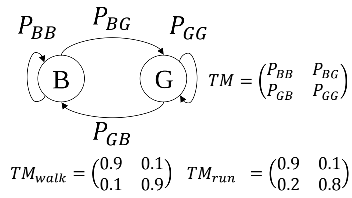

Figure 7: The state diagram and transition matrices of GE model during walking and running

persistence. That is, the channel tends to remain in the same state for longer periods before transitioning to a different state. To estimate $P_{ij}^c(t)$ $(i, j \in \Omega = \{G, B\})$, GE uses the equation below:

$$P_{ij}^c = \underbrace{P_{ii} \times P_{ii} \times P_{ii} \times \dots P_{ii}}_{\text{c-1 times}} \times P_{ij} \tag{3}$$

where P_{ii} and P_{ij} are obtained from TM.

GE model is unable to remember history and, thus, is not reliable in long-term channel prediction. This is elaborated upon in Section IV-C. Hence, the Extended GE model (EGE) was proposed in [25] to remember the channel history. As illustrated in Fig. 8, the major difference between GE and EGE is that EGE has internal sub-states. Therefore, EGE has two types of transitions: intra-transitions and inter-transitions. For instance, if the channel transits to the G state from the B state, it transits to the first sub-state in the G state (i.e., G_1). If the next channel state is G, an intra-transition occurs, and the channel transits to the second sub-state in the G state (G_2). After observing the G state for n consecutive times, if a B state is observed, the channel transits from the n^{th} sub-state in the G state to the first sub-state in the B state, i.e., transits from G_n to B_1. In other words, assuming each state i has m internal sub-states, the sub-state i_r represents the r^{th} successive observation in state i. Hence, EGE can represent different state-durations given a sufficient number of internal sub-states. EGE estimates $P_{ij}^c(t)$ using the equation below:

$$P_{ij}^c = P_{i_1 i_2} \times P_{i_2 i_3} \times P_{i_3 i_4} \times \dots P_{i_{c-1} i_c} \times P_{i_c j_1} \tag{4}$$

As it will be discussed in Section IV-C EGE compensates the inaccuracy of GE in long-term channel prediction by leveraging a considerable amount of sub-states which imposes unaffordable memory complexity.

B. Improved GE (IGE) Model

To sustain the advantage of EGE on prediction accuracy but overcome its drawback on complexity, we propose a new channel model that takes the normal distribution of state-durations into account for better channel prediction. As demonstrated earlier in Fig. 4, the behavior of $P_{ij}^c(t)$

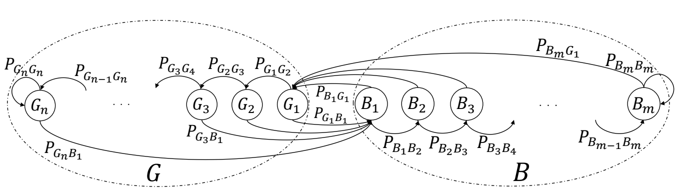

Figure 8: Extended GE model.

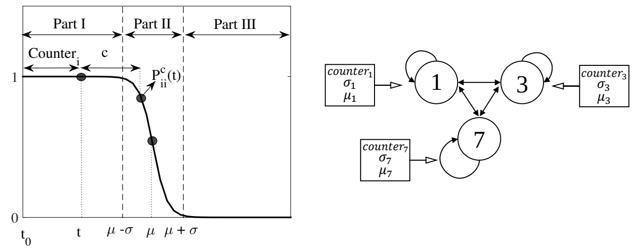

(a) (b)

Figure 9: IGE model: (a) P_{ii}^c variation trend; (b) IGE diagram.

exhibits an "S-shaped" pattern. Drawing inspiration from this observation, we can partition $P_{ij}^c(t)$ for cases where $j = i$ into three distinct segments, as shown in Fig. 9(a). These segments are determined based on the values of μ_i and σ_i, where μ_i and σ_i denote the mean and standard deviation of the i-state-durations, respectively. $P_{ii}^c(t)$ is approximately 1 in Part I and almost 0 in Part III. The transition occurs in Part II, in which $P_{ii}^c(t)$ is decreased exponentially before μ_i and logarithmically after μ_i. This observation also reveals that the trend of $P_{ij}^c(t)$ for the case $j = i$ has the reverse trend to that of the Cumulative Distribution Function (CDF) of the length of i-state-durations. The trend of CDF of a normal distribution can be described by its mean and its standard deviation. Thus, to predict the trend of $P_{ij}^c(t)$, the GE model is extended by associating the following three parameters with each state i: μ_i, σ_i, and $counter_i$ (Fig. 9(b)). $counter_i$ represents the length of the current i-state-duration, which is similar to the sub-states in EGE and is reset to zero after each inter-transition. For example, if the channel moves to state i from state j, $couter_j$ is reset to zero but $counter_i$ is set to 1. If the next channel state is i, $counter_i$ is increased by 1. After each inter-transition, μ_i and σ_i are updated as follows:

$$\mu_i = \omega \times counter_i + (1 - \omega) \times \mu_i, \tag{5}$$

$$\sigma_i = \omega \times |counter_i - \mu_i| + (1 - \omega) \times \sigma_i, \tag{6}$$

where ω is a weighting factor. Please note, since these variables are not included in the TM, adding them to the model does not add memory to the process and thus does not make the random process non-Markovian. Fig. 9(b) gives an example of IGE with 3 states (for 3 favorable power levels: 1, 3, and 7). In what follows, we develop a new function to estimate $P_{ij}^c(t)$ using the IGE model.

Considering that the trend of $P_{ij}^c(t)$ for the case $j = i$ has the reverse trend to that of CDF of the length of i-state-duration and following the formula for the CDF of the normal distribution, we model $P_{ii}^c(t)$ as follows:

$$P_{ii}^c(t) = 1 - CDF(\mu_i, \sigma_i, c + counter_i) = 1 - \frac{1}{\sigma_i\sqrt{2\pi}} \sum_{k=0}^{c-1} \exp - \frac{(k + counter_i - \mu_i)}{2\sigma_i^2}. \tag{7}$$

Accordingly, $P_{ij}^c(t)$ with $j \neq i$ can be rewritten based on the chain rule of conditional probability as below:

$$P_{ij}^{c}(t) = \underbrace{P_{ii}^{c-1}(t)}_{\text{A}} \times \underbrace{P(x_{t+c} = j | x_t = \cdots = x_{t+c-1} = i \wedge x_{t-1} \neq i)}_{\text{B}} \quad (8)$$

where part A calculates the probability of being in state i from frame t to frame $t+c-1$. It is determined using Eq. (7). Part B computes the transition probability from state i to state j at frame $t+c$. In what follows, we discuss how to calculate part B. We first rewrite P_{ii}^{c} based on the chain rule of conditional probability:

$$P_{ii}^{c}(t) = P_{ii}^{c-1}(t) \times P(x_{t+c} = i | x_t = \cdots = x_{t+c-1} = i \wedge x_{t-1} \neq i).$$

Thus:

$$P(x_{t+c} = i | x_t = \cdots = x_{t+c-1} = i \wedge x_{t-1} \neq i) = \frac{P_{ii}^{c}(t)}{P_{ii}^{c-1}(t)}.$$

On the other side, the probability of leaving state i at $t+c$ given that the channel has been in the state i from t to $t+c-1$ can be calculated as below:

$$\begin{aligned}&\sum_{\substack{j \in \Omega \\ j \neq i}} P(x_{t+c} = j | x_t = \cdots = x_{t+c-1} = i \wedge x_{t-1} \neq i) \\ &= 1 - P(x_{t+c} = i | x_t = \cdots = x_{t+c-1} = i \wedge x_{t-1} \neq i) \\ &= 1 - \frac{P_{ii}^{c}(t)}{P_{ii}^{c-1}(t)}.\end{aligned}$$

Therefore, the probability of transiting to a *specific* new state $j \neq i$ (i.e., part B) can be calculated as follows:

$$\begin{aligned}P(x_{t+c} =& j | x_t = \cdots = x_{t+c-1} = i \wedge x_{t-1} \neq i) = \\ &\left(1 - \frac{P_{ii}^{c}(t)}{P_{ii}^{c-1}(t)}\right) \times \frac{P_{ij}}{1 - P_{ii}}\end{aligned} \quad (9)$$

where both P_{ij} and P_{ii} are derived from the transition matrix and represent the transition probability from state i to the state j, and the probability of a self-transition at state i, respectively. Based on Eq. (9), Eq. (8) can be written as

$$\begin{aligned}P_{ij}^{c}(t) &= P_{ii}^{c-1}(t) \times \left(1 - \frac{P_{ii}^{c}(t)}{P_{ii}^{c-1}(t)}\right) \times \frac{P_{ij}}{1 - P_{ii}} \\ &= \left(P_{ii}^{c-1} - P_{ii}^{c}\right) \times \frac{P_{ij}}{1 - P_{ii}}.\end{aligned} \quad (10)$$

C. Comparative Analysis of GE, EGE, and IGE

In this section, we present a comparative analysis of the established GE and EGE models, alongside our proposed IGE model. To facilitate this comparison, we conducted a series of simulations using collected RSSI samples. These simulations help us to better understand how each model performs in predicting channel quality over an extended period. Fig. 10 illustrates the GE model's estimations for $P_{ij}^{c}(t)$ in scenarios of walking and running, specifically for the case where $j = i$ (denoted as $P_{ii}^{c}(t)$). $P_{ij}^{c}(t)$ for $j \neq i$ has not been shown as it has the reverse trend to that $P_{ii}^{c}(t)$, as demonstrated in Fig. 4(b). By comparing with Fig. 4(a), it can be seen that

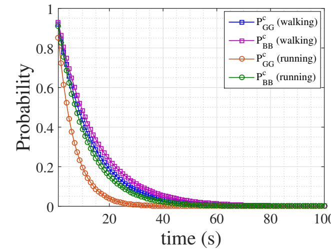

Figure 10: Estimated P_{GG}^{c} and P_{BB}^{c} by GE model.

there is a big difference between the P_{ii}^{c} predicted by the GE model and that calculated based on the real observations. That is, the GE model can effectively predict the probability of channel state transitions for the next one or two frames, but its long-term predictions are highly inaccurate. The key reason is that the length of the state-duartions does not match an exponential distribution. In other words, in the GE model, the state of the channel at the next frame depends only on the state at the current frame and the transit probabilities, and not on the channel history. For example, the TMs of the following two sample blocks 'GGBBBBGGGGGGBBBB' and 'GGGGBBGGGGBBBBBB' are the same but their pattern (i.e., their state-duration) are different. Due to this memoryless property, $P_{ij}^{c}(t)$ estimated by the GE model doesn't match with the one presented in Fig. 4(a).

The EGE model was developed to address the lack of a memory component in the GE model, while still preserving its essential Markovian property. Since the channel fluctuation in the periodic dynamic postures (e.g., in the walking) behaves like a periodic random process, the sufficient number of sub-states in EGE depends not only on the frame rate but also on the fluctuation period (in terms of the number of channel observations). In other words, if the number of sub-states in EGE is not smaller than the largest state-duration, EGE can model the behavior of the periodic random process.

A gait cycle usually takes about 1 second because the average number of steps in walking is about 116 steps per minute [36]. Since the availability of the LoS path is changed during one gait cycle (see Fig. 1), at the rate of 20 frames per second, EGE requires at least 20 sub-states per each state. To demonstrate the influence of sub-state quantity on EGE performance, we have employed EGE to model channel behavior during both walking and running activities using

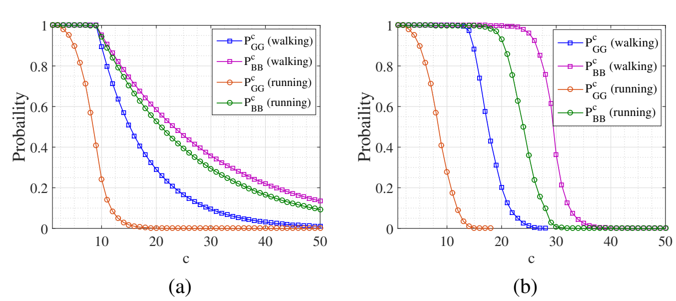

Figure 11: P_{GG}^{c} and P_{BB}^{c} with EGE: (a) $m = 10$, and (b) $m = 50$.

two distinct sub-state configurations: (a) 10 sub-states, falling below the minimum required quantity, and (b) 50 sub-states, ensuring an ample sub-state count.

Fig. 11 shows the P^c_{GG} and P^c_{BB} estimated by EGE with 10 and 50 sub-states. As anticipated, the accuracy of EGE is contingent upon the number of sub-states. Specifically, a greater number of states leads to enhanced estimation accuracy. However, EGE's major drawback is the high memory complexity, $O(|\Omega|^2m^2)$, where $|\Omega|$ and m are the number of general states and sub-states per general state, respectively. In contrast to EGE, IGE exhibits reduced memory complexity, falling within the same order of magnitude as the GE model. Specifically, the memory complexity of IGE is now at $O(|\Omega|^2 + 3 \times |\Omega|)$.

Following the preceding discussion, we carried out simulations to assess the accuracy of the proposed model. Fig. 12 illustrates that the predicted trend of $P^c_{ii}(t)$ using the proposed model is very similar to its real trend. Hence, the proposed model can estimate the long-term channel transition accurately. Section VI-B further examines the influence of the models under discussion on the performance of the proposed communication protocol.

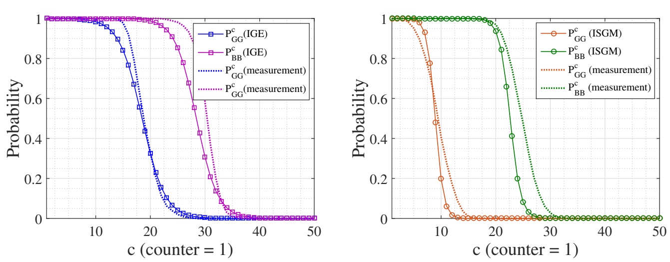

(a) (b)

Figure 12: Estimated P^c_{GG} and P^c_{BB} by IGE model compared with real measurements (a) walking (b) running.

V. The Protocol Design of ATPS

In this section, we present the development of the proposed ATPS protocol. Initially, we provide an overview of the system setup specific to WBANs, adhering to IEEE standards. Based on this standard, we investigate the intricacies of the ATPS protocol, focusing particularly on the methodology for adjusting transmission power levels according to channel predictions. The section then progresses to introduce a novel scheduling algorithm designed to optimize transmission costs. That is, instead of immediate transmission, the sending node considers the option of postponing its transmission if the channel quality is predicted to become better. This is achieved by strategically selecting the most suitable time frame for transmitting packets. Central to this algorithm is its ability to adapt to channel variations and accurately predict the likelihood of being in a specific channel state at a given future moment. In what follows, we explain different steps of building the ATPS communication protocol.

A. Communication Setup

Consider a WBAN composed of several sending nodes and a gateway where the sending nodes communicate with the gateway directly in a one-hop star topology. Fig. 13 shows a TDMA-based MAC setup for WBANs following IEEE standards [1], [2]. In this setup, time is divided into frames, and the start of each frame is announced using a beacon packet transmitted by the gateway. Each frame includes a CFP (contention-free period) and a CAP (contention access period). The CFP includes n time slots (where n is the number of sending nodes) and each time slot is pre-allocated to a specific sending node in WBAN through which intra-WBAN collisions are avoided. CFP's objective is to provide each node with an exclusive opportunity to transmit at least one packet within a frame without contending with others. However, a node may choose not to utilize this opportunity due to unfavorable channel conditions, resulting in packet buffering.

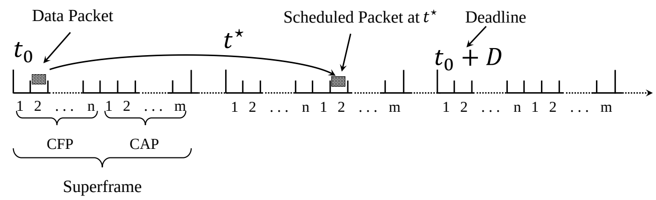

Figure 13: Illustration of packet scheduling

The CAP consists of m time slots. In these slots, those sending nodes that have extra packets compete with each other to access the channel following a slotted CSMA/CA algorithm. Since bursty transmission is permitted, any sending node with packets in its buffer will compete for every available time slot in CAP. This continues until either its buffer is empty or there are no more time slots unless the channel conditions are unfavorable. Note that each time slot is assumed to be long enough to allow transmitting a data packet and receiving its corresponding ACK packet.

ALGORITHM 1: Proposed ATPS

Input : RSSI of beacon packet and channel model properties at t_0 ($I(t_0)$)

$p \leftarrow$ packet generated at t_0;
$retrans\_count \leftarrow 0$;
do
  $i \leftarrow channel(t_0)$; /* select power based on the estimated channel state */
  $send(p, i)$; /* send packet p using power level i */
  if *ACK is received* **then**
    $rssi \leftarrow RSSI(ACK)$;
    find the real channel state based on the measured rssi;
    update channel model properties;
    break;
  $retrans\_count = retrans\_count + 1$
  update channel model properties;
while $retrans\_count < retrans\_threshold$;

This article has been accepted for publication in IEEE Internet of Things Journal. This is the author's version which has not been fully edited and content may change prior to final publication. Citation information: DOI 10.1109/JIOT.2024.3355702

B. Adaptive Transmission Power Selection (ATPS)

Algorithm 1 shows the procedure of the proposed ATPS at each sending node. When the beacon packet is received, the sending node measures its RSSI and checks the channel state following the channel symmetry and using the current channel state information provided by the channel model (e.g., GE, EGE, or IGE). Since each state i ($i \in \{1, 3, 7\}$) represents a channel state for which power level i is the best power level for communication, the sending node can select the corresponding power level based on the channel estimation (line 4). Once the channel state is estimated and the power level is selected, the packet is transmitted using the selected power level (line 5). Since the time difference between sending a packet and receiving its ACK packet is short, it is reasonable to assume that the channel does not change during a time slot. Due to channel symmetry, the ACK packet can be sent back to the sending node using the same power level. To this end, the sending node should include its transmit power level in the packet. However, the focus of this paper is on reducing the battery usage of the sending node, and we assume the battery of the gateway can be easily replaced or recharged. Hence, to avoid complexity and overhead, we assume ACK packets are always transmitted by power level 7. After measuring the RSSI of the received ACK packet, following the Markov models described in Section III, the transition probabilities are updated for future channel estimation. In case the ACK packet is not received, the sending node assumes the channel quality is worse than its estimation. Thus, it makes another estimation among the states related to the lower channel quality. If retransmission is enabled, the sending node repeats all steps mentioned above.

Since channel quality in WBANs changes over time due to body movements, it just wastes energy to transmit packets when the channel quality is bad. In many applications of WBANs, packet transmission can tolerate some delay. Hence, energy can be saved by postponing the packet transmission until the channel becomes good. Motivated by this, we present a transmission scheduling policy to save energy, reduce interference, and improve communication reliability. To learn the channel variation pattern, the sending nodes benefit from the discussed channel prediction models (GE, EGE, or IGE). Since the channel does not drastically vary in a few tens of milliseconds even when the subject is running, it is assumed that the channel is stable during a frame.

C. Scheduling-Enabled ATPS

Algorithm 2 shows the pseudo-code of the proposed scheduling-enabled ATPS. Note that the scheduling algorithm is independently executed by every single sending node. Consider a sending node where a newly generated packet at frame t_0 should be transmitted within the next D frames, as illustrated in Fig. 13. The idea of scheduling is to find the best frame $t^\star$ ($t_0 \le t^\star \le t_0 + D$) where the transmission cost is minimum (lines 3-12). To this end, the following function is defined to explore the average transmission cost at frame $t_0 + t$ (where $0 < t \le D$):

ALGORITHM 2: Scheduling enabled ATPS

Input : channel model properties at frame t_0 ($I(t_0)$)

1 $p \leftarrow$ packet generated at t_0;
2 $retrans\_count \leftarrow 0$;
3 $t^\star = t_0 + 1$;
4 **for** $t = 1, \ldots, D$ **do**
5 $\quad C(t_0 + t, I(t_0)) = 0$;
6 $\quad$ **for** $j = 1, \ldots, |\Omega|$ **do**
7 $\quad\quad C(t_0 + t, I(t_0)) += P(t_0, i, t_0 + t, j, c) \times cost_j$;
8 $\quad$ **if** $C(t_0 + t, I(t_0)) < C(t^\star, I(t_0))$ **then**
9 $\quad\quad t^\star = t_0 + t$;
10 schedule p to be sent at $t^\star$;
11 $channel(t_0) \leftarrow$ estimated channel state at frame t_0;
12 **if** *packet is available to be sent at* t_0 **then**
13 $\quad p \leftarrow$ packet scheduled to be sent at t_0;
14 $\quad$ **do**
15 $\quad\quad i \leftarrow channel(t_0)$; /* select power level */
16 $\quad\quad send(p, i)$; /* send with power level i */
17 $\quad\quad$ **if** *ACK is received* **then**
18 $\quad\quad\quad r_i = \omega \times r_i + (1 - \omega)$;
19 $\quad\quad\quad rssi \leftarrow RSSI(ACK)$;
20 $\quad\quad\quad channel(t_0) \leftarrow$ real channel state at t_0 that is determined based on rssi;
21 $\quad\quad\quad break$;
22 $\quad\quad r_i = \omega \times r_i$;
23 $\quad\quad retrans\_count = retrans\_count + 1$
24 $\quad\quad update\ model\ properties$;
25 $\quad\quad channel(t_0) \leftarrow$ estimated channel state at t_0;
26 $\quad$ **while** $retrans\_count < retrans\_threshold$;

$$C(t_0 + t, I(t_0)) = \sum_{j \in \Omega} P(t_0, i, t_0 + t, j, c) \times cost_j \qquad (11)$$

where $cost_j$ represents the transmission cost using power level j and is calculated using Eq. (2). $I(t_0)$ is the information about the channel variation pattern at frame t_0, including the mean and the variance of state-duration of each state i (i.e., μ_i and σ_i). c represents the length of the current state-duration in the current channel state i. $P(t_0, i, t_0 + t, j, c)$ shows the probability of being in state j at $t_0 + t$, given that the channel state at t_0 is i and c consecutive samples in this state has been observed. To calculate the transmission cost at each channel state j, the PDR of communication at this channel state is needed. r_j is defined as the average PDR at channel state j. Since each sending node doesn't know the communication reliability of different power levels at the beginning, r_j is set to 1. Then, r_j is updated after each transmission in state j as below (lines 18 and 22):

$$r_j = \omega \times r_j + (1 - \omega) \times ACK \qquad (12)$$

where $0 \le \omega \le 1$ is the weighting factor and ACK is 1 if the packet is delivered and 0 if the packet is lost. Once the transmission cost at each frame is calculated, the packet is scheduled to be sent at the best frame ($t^\star$) which is the frame with the minimum expected transmission cost. The minimum expected transmission cost and the corresponding transmission time ($t^\star$) are defined as below:

$$C(t^\star, I(t_0)) = \min_{t=0}^{D} C(t_0 + t, I(t_0)) \tag{13}$$

To calculate Eq. (11) at each frame t, $P(t_0, i, t_0 + t, j, c)$ needs to be calculated using the equation below:

$$P(t_0, i, t_0 + t, j, c) = \sum_{k \in \Omega} P(t_0, i, t_0 + 1, k, c) \times P(t_0 + 1, k, t_0 + t, j, c') \tag{14}$$

where $P(t_0, i, t_0+1, k, c)$ is equal to P^c_{ik}, which is calculated using Eq. (7) or (10). c' is the length of state-duration in the channel state at the next frame. Therefore, it is 1 if the next channel state is new ($i \neq k$); otherwise, it is $c + 1$. As soon as $t^\star$ is calculated, the packet is buffered until its scheduled release frame. In each frame, the sending node checks the buffer for any scheduled packet to be sent (line 12). If there is a packet, the sending node transmits the packet and listens to the channel for the ACK packet. If the ACK packet is received, its RSSI is measured, the reliability of communication using the selected power level is updated, and the real channel state is determined (lines 17-21). Otherwise, if the packet(s) is lost, the sending node finds it has overestimated the channel quality, and thus, it updates the current channel state to a new higher level. In case there is no packet to send, the sending node evaluates its internal channel model to make predictions. Therefore, it updates the channel states based on its estimation as it is impossible to get the real channel state without communication.

D. Efficient calculation of channel transition probabilities using dynamic programming

As can be seen from Eq. (14), $P(t_0, i, t_0 + t, j, c)$ is calculated on a recursive basis that takes $t - 1$ steps. At each step t', $|\Omega|^{t'}$ new components are generated. The total number of components to be calculated is:

$$|\Omega| + |\Omega|^2 + |\Omega|^3 + \cdots + |\Omega|^{t-2} + |\Omega|^{t-1} = \frac{|\Omega|^t - 1}{|\Omega| - 1} - 1 \tag{15}$$

According to Eq. (15), the time complexity of recursively calculating $P(t_0, i, t_0 + t, j, c)$ is $O(|\Omega|^t)$. Many of the recursive components have the same results which indicate a potential to calculate each component only once and then reuse the results. Motivated by this, instead of using a recursive approach, a dynamic programming solution is designed to remember intermediate results and reuse them through which, the time complexity of calculating $P(t_0, i, t_0 + t, j, c)$ is extremely reduced. It can be seen that in each step only half of the components (generally, only $|\Omega| \times t_0$ components) need to be calculated. Therefore, generally, the total number of the required components to be calculated to find $P(t_0, i, t_0+t, j, c)$ using dynamic programming is:

$$|\Omega| + 2 \times |\Omega| + 3 \times |\Omega| + \cdots + (t-1) \times |\Omega| = \frac{t \times (t-1) \times |\Omega|}{2} \tag{16}$$

Thus, the time complexity of calculating $P(t_0, i, t_0 + t, j, c)$ using the dynamic programming solution is reduced to $O(|\Omega| \times t^2)$. Algorithm 3 gives the pseudocode of calculating

ALGORITHM 3: Calculation of $P(t_0, i, t_0 + t, j, c)$ using dynamic programming

1 **Function:** P($t_0, i, t_0 + t, j, c$)
2 **for** $\tau = t - 1, \ldots, 0$ **do**
3   **for** $k = 1, \ldots, |\Omega|$ **do**
4   **if** $\tau == t - 1$ **then**
5   **if** $k == i$ **then**
6   **for** $c' = 1, \ldots, \tau - 1, c + \tau$ **do**
7           $P(t_0 + \tau, k, t_0 + t, j, c') = P^{c'}_{kj}$;
8   **else**
9   **for** $c' = 1, \ldots, \tau$ **do**
10           $P(t_0 + \tau, k, t_0 + t, j, c') = P^{c'}_{kj}$;
11   **else**
12   **if** $k == i$ **then**
13   **for** $c' = 1, \ldots, \tau - 1, c + \tau$ **do**
14           $P(t_0 + \tau, k, t_0 + t, j, c') = P(t_0 + \tau + 1, k, t_0 + t, j, c' + 1)$;
15   **for** $kk = 1, \ldots, k-1, k+1, \ldots, |\Omega|$ **do**
16             $P(t_0 + \tau, k, t_0 + t, j, c') += P(t_0 + \tau + 1, kk, t_0 + t, j, 1)$;
17   **else**
18   **for** $c' = 1, \ldots, \tau$ **do**
19           $P(t_0 + \tau, k, t_0 + t, j, c') = P(t_0 + \tau + 1, k, t_0 + t, j, c' + 1)$;
20   **for** $kk = 1, \ldots, k-1, k+1, \ldots, |\Omega|$ **do**
21             $P(t_0 + \tau, k, t_0 + t, j, c') += P(t_0 + \tau + 1, kk, t_0 + t, j, 1)$;

$P(t_0, i, t_0 + t, j, c)$ using dynamic programming. As can be seen, the first loop (line 2-21) calculates the components from the last step ($t - 1$) where the components can be directly calculated by Eqs. (7) and (10). Using this loop, the components in the higher step are available at the beginning of each step. In each step represented by τ, there is another loop (line 3-21) where the probability of transition from each channel state $k \in \{1, \ldots, |\Omega|\}$ to state j within the next $t - \tau$ frames is considered. In this loop, different transition probabilities are calculated depending on the current and the next channel state, and the length of state-duration (lines 6-7, 9-10, 12-16, and 18-21) are stored for further reuse. Note that, since D and $|\Omega|$ are usually very small, finding $t^\star$ will not incur a large overhead to the sending node.

VI. Experimental Evaluation

This section evaluates the performance of ATPS under the use of the discussed channel models first. Then, we compare IGE-enabled ATPS with the state-of-the-art schemes through several experiments based on the following three metrics:

- **Power level usage**: the number of transmissions under each power level is measured, by which the distribution

This article has been accepted for publication in IEEE Internet of Things Journal. This is the author's version which has not been fully edited and content may change prior to final publication. Citation information: DOI 10.1109/JIOT.2024.3355702

of power level used for all implemented schemes can be compared. Since it is impossible to perform quantitative measurement of the real interference produced by the packet transmissions, this metric allows a comparison of the interference generated by different schemes in a relative way since the more the number of transmissions using a high transmission power, the larger the probability to produce more interference.

- **Energy consumption**: since the gateway is generally a device such as a smartphone that is commonly recharged regularly, the total energy spent on packet transmission is measured at the sending node side.
- **Packet loss rate**: the ratio of the number of lost packets to the total number of transmitted packets.

A. Experiment Setup

We adopt the same setup as presented in Fig. 1 with the sending node attached to the wrist and the gateway mounted on the chest. However, since the proposed scheme is executed locally by the sending node, extra nodes can be added to the network without sacrificing the performance of the communication scheme. This setup has also been adopted in much other research works [30], [9], [37], [26] because (1) in many applications, body sensors tend to be embedded into the user's wrist watch or fancy wrist bands; (2) the shoulder joint is the most mobile joint and can provide a wide range of movements for the wrist in combination with the elbow joint. Hence, the location of the sending node and consequently the channel to the gateway is highly unstable, making the channel estimation very challenging. Without loss of generality, we limit the transmit power levels to levels 1, 3, and 7 as they are enough for reliable and energy-efficient communication [9]. The size of data packets and ACK packets is set to 41 bytes and 13 bytes, respectively. The packets are generated at a constant rate of 0.1 pkt/s for low data rate applications (e.g., monitoring blood pressure) and 20 pkt/s for high data rate applications (e.g., EMG monitoring), respectively, and then can be transmitted to the gateway according to a predefined TDMA schedule. However, burst transmission is allowed. That is, the sending node can transmit a couple of buffered packets in a single superframe. Three participants were asked to stay in the following postures, with each one lasting for 30 minutes:

- **Sitting with folded hand**: the distance between the sending node and the gateway is only a few centimeters. This covers postures where the hand is close to the chest, e.g., eating, drinking, brushing teeth, etc.
- **Standing upright**: the thumb is parallel to the trousers so that the sending node is close to the side pocket and the LoS path to the gateway is blocked.
- **Walking**: in this posture, the LoS path between transceivers is regularly connected/disconnected. It is a good scenario to consider how different channel models can predict quick channel fluctuations.
- **Running**: in this scenario, the channel quality varies very fast. It can be used to test the performance limits of different models.

In static postures such as sitting and standing, the channel quality is constant over time, and postponing the transmission has no impact on communication performance. In dynamic postures (e.g., walking and running), due to the frequent channel fluctuation, the LoS is blocked during part of a gait cycle and is available for the rest of the cycle. Since the average number of steps in walking is about 116 steps per minute [36], a one-second transmission deadline provides a significant potential for the sending node to reduce the transmission cost by postponing the transmissions. Note that, since the channel is changing periodically, taking the deadline more than 1 second does not significantly influence the performance of the transmission schemes.

In the first set of experiments, the performance of the proposed IGE model is compared with the GE and EGE models. To this end, three separate versions of the ATPS protocol are developed, each of which uses one of the discussed channel models. For the sake of simplicity, each version of the ATPS protocol is named based on the channel model it uses. All models (GE, EGE, and IGE) have 3 channel states. Each state in the EGE model contains 20 internal states. Hence, the size of the transition matrix in the GE, IGE, and EGE models is limited to 18 bytes, 36 bytes, and 7.2 kilobytes, respectively. In the second set of experiments, the performance of IGE-enabled ATPS is compared with the state-of-the-art schemes such as Experio [26], Chimp [9], and Tuatara [30]. To provide reliable communication, retransmission at the MAC sub-layer is enabled. Hence, the sending node retransmits lost packets up to 15 and 3 times at the low and high data rate scenarios, respectively. To ensure fair comparison among all schemes, it is essential to repeat the simulations under identical conditions. To this end, a two-phase RSSI collection method is utilized [9].

B. ATPS Under Different Channel Models

In this section, the performance of ATPS under the use of three channel prediction models (GE, EGE, and IGE) is evaluated. The transition matrix is created based on the collected RSSI traces and is updated following the aging method [38]. The simulation results show that ATPS delivers all packets under all models in all scenarios (sometimes after multiple retransmissions). Hence, results on packet loss rate are not included. To simplify the explanation, we discuss the results in two groups: *static* and *dynamic* postures.

1) Static Postures: In static postures, the channel state is mainly constant over time and accurate long-term channel prediction is not much of importance. Hence, as is also illustrated in Fig. 14, the performance of all models is relatively similar. For example in sitting and at the packet rate of 0.1 pkt/s, the GE, IGE, and EGE models use power level 1 for more than 90%, 96%, and 97% of the transmissions, respectively. Increasing the packet rate to 20 pkt/s further reduces the difference between schemes since more channel feedback is provided for all models. Due to the similar trend in the usage of power levels, they consume roughly the same amount of energy.

In standing, the LoS path to the gateway is blocked by the body trunk and the channel is mainly in state 3. In a low packet

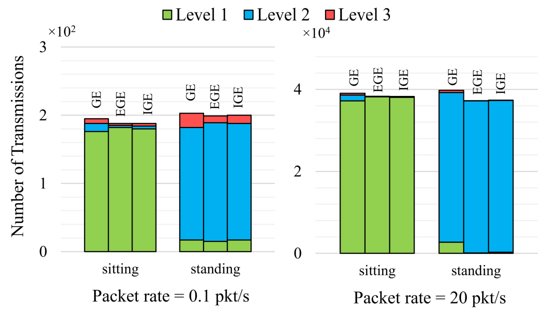

(a) Power level usage

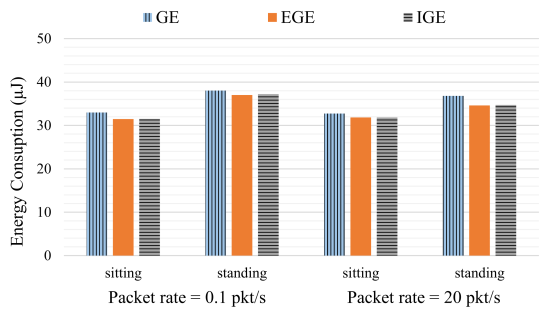

(b) Energy consumption

Figure 14: Experiments for static postures under packet rate of 0.1 pkt/s and 20 pkt/s.

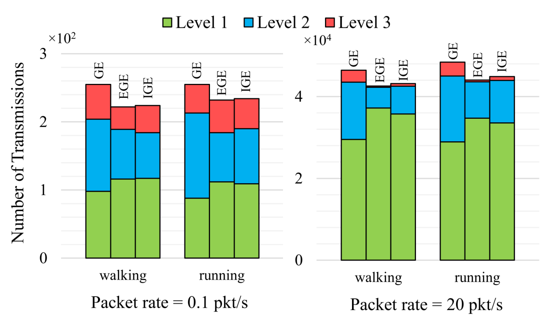

(a) Power level usage

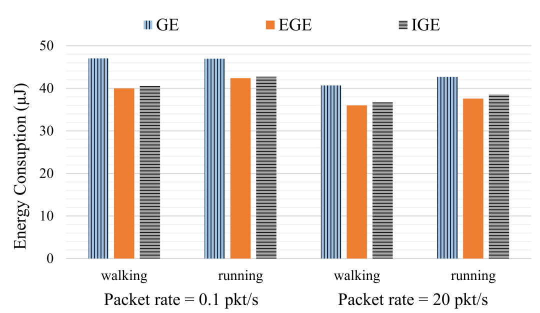

(b) Energy consumption

Figure 15: Experiments for dynamic postures under packet rate of 0.1 pkt/s and 20 pkt/s.

rate scenario, GE, IGE, and EGE use power level 3 for more than 80%, 85%, and 87% of transmissions, respectively. As is expected, at the rate of 20 pk/s the usage of power level 3 is reached to 92% in GE and more than 99% in IGE and EGE. Accordingly, the per packet energy consumption of the GE model is only 3% and 6.3% more than that of the EGE model, in low and high packet rate scenarios, respectively, while the IGE and EGE models consume almost the same amount of energy. In all models, most of the packets are delivered at their first transmission. Hence, there are not many retransmissions.

2) Dynamic Postures: Analyzing the RSSI traces during walking and running shows that the channel commonly transits between states 1 and 3. Due to the rapid channel fluctuation in dynamic postures, predicting the channel state is challenging. Hence, there are situations where the channel is predicted to be in state 1 while it is in state 3, and vice versa. This is a common problem with the GE model, while IGE and EGE can accurately predict the channel state, particularly in the high packet rate scenarios. This is because the GE model is memoryless and cannot remember for how many frames the channel has been in one state before transiting.

As is shown in Fig. 15(a), unlike the GE model, the distribution of usage of power levels in IGE and EGE are almost the same. They use power level 1 for most of their transmissions, particularly when the packet rate is high. For example, at 20 pkt/s, the IGE and EGE models use power level 1 for more than 82% and 87% of their transmissions in the walking, 20% more than that of the GE model. On the other hand, in the same scenario, the GE model uses power level 7 for 6.2% of its transmission, while the figures for IGE and EGE are 1.4% and 0.7%, respectively. Accordingly, GE consumes more energy than EGE and IGE, between 11% in the running to up to 17% in the walking (see Fig. 15(b)). The simulation results confirm that the proposed IGE model outperforms the GE model and nearly performs as well as the EGE model while using less memory.

C. Comparing ATPS with other Schemes

To evaluate the performance of the proposed IGE-enabled ATPS, it is compared with state-of-the-art schemes, including:

- DPPI [18], Experio [26], Chimp [9], and Tuatara [30]: these schemes have been described in detail in Section II.
- FLP (Fixed Low Power) and FHP (Fixed High Power): regardless of the channel state FLP always uses the lowest power level (level 1), whereas FHP always uses the highest power level (level 7).
- Optimal: it is simulated over the collected RSSI samples. In this scheme, the sending node knows the instant and the long-term RSSI value before transmitting a packet. Hence, it can always select the best transmission time. Since this scheme provides the best performance, we use it as a baseline to assess the other schemes.

Fig. 16 shows the results of the experiments. Since retransmission is enabled, transmission schemes differ in the total number of transmissions. It turns out that the obtained experimental data is highly skewed with many small values and a few large values. To display the small values, the large values are allowed to cut through the plot area and then, they are labeled with the real values.

1) Static Postures: In sitting scenarios, power level 1 is the optimal choice for the majority of transmissions. This is supported by simulation results, where the Optimal scheme predominantly utilizes power level 1. ATPS, FLP, Chimp, and

This article has been accepted for publication in IEEE Internet of Things Journal. This is the author's version which has not been fully edited and content may change prior to final publication. Citation information: DOI 10.1109/JIOT.2024.3355702

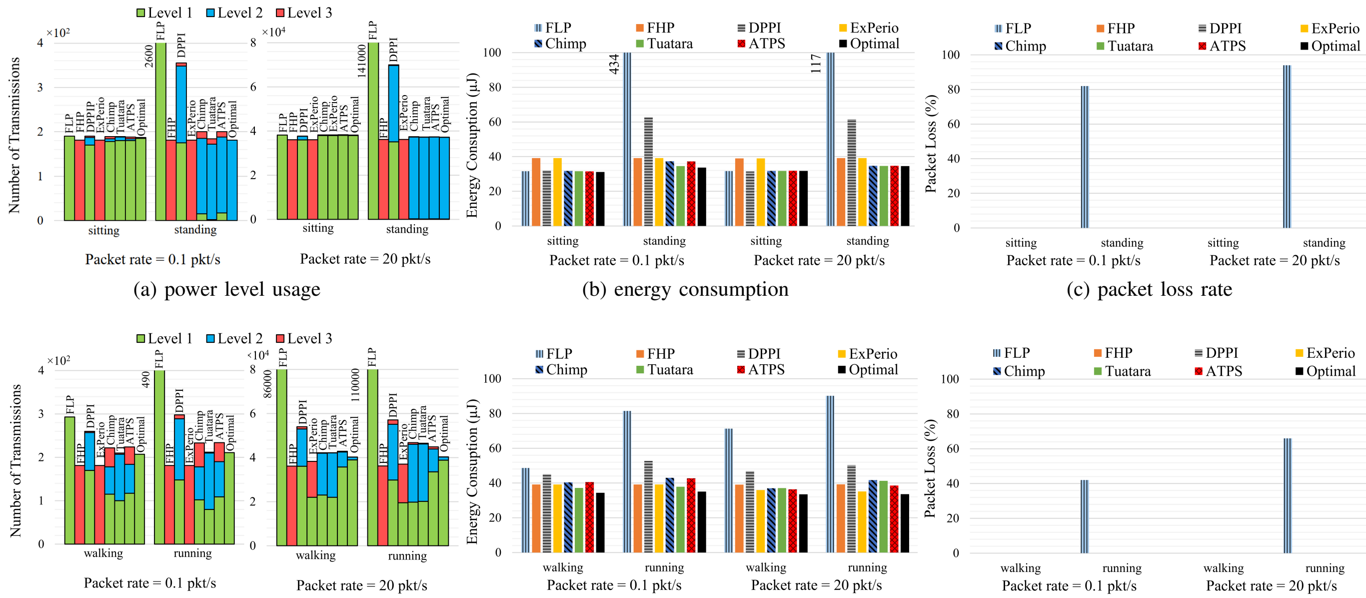

(a) power level usage (b) energy consumption (c) packet loss rate

(d) power level usage (e) energy consumption (f) packet loss rate

Figure 16: Experiments under different data rates: (a), (b) and (c) show the results for static postures; (d), (e) and (f) show the results for dynamic postures.

Tuatara exhibit similar performance to the Optimal scheme, especially in high packet rate scenarios. These schemes deliver most of the packets at their first transmission, resulting in comparable energy consumption. DPPI uses power level 1 for more than 90% and power level 3 for about 7% of its transmissions on average. While not efficient, DPPI outperforms FHP and ExPerio significantly.

ATPS performs similarly to the Optimal scheme in standing scenarios, especially at high data rates, with power level 3 used for over 99% of its transmissions and only a 0.5% increase in energy consumption compared to the Optimal scheme. Similarly, Tuatara and Chimp exhibit performance closely aligned with the Optimal scheme, with improved performance at higher packet rates. They achieve full packet delivery while minimizing the use of power level 7, even at low packet rates. FLP's approach of retransmitting lost packets with power level 1 leads to numerous transmissions and significant energy overhead, delivering only a small fraction of packets. DPPI suffers from the ping-pong effect [9], resulting in a high number of retransmissions and substantial energy usage.

When there is no periodicity in the movement pattern of the subject (e.g., in static postures), ExPerio behaves the same as FHP. That is, regardless of the packet rate (and the body posture), they use power level 7 for all transmissions. Hence, they produce the highest potential interference and consume up to 25% more energy than ATPS.

D. Dynamic Postures

As already mentioned, during walking and running the channel mainly alternates between states 1 and 3. Hence, ATPS buffers the packets when the channel is at state 3 and transmits them when the channel transits to state 1. For example in walking and running, as is shown in Fig. 16, ATPS uses power level 1 for about 85% and 75% of transmissions, respectively, when the packet rate is high. Except for the Optimal scheme, ATPS is the most and the second most energy-efficient scheme for walking and running, respectively. However, at a low packet rate, due to the lack of initial information about the channel pattern and the low rate of channel feedback, power level 1 is used for only 50% of the transmissions. Chimp behaves like ATPS at low packet rate scenarios and has a similar trend on power level usage. Tuatara rarely uses power level 7, particularly because of its knowledge of the real-time location of the sending node relative to the gateway. Its total number of transmissions is 10% less than that of ATPS, so it can save more energy, however, at the cost of extra hardware (i.e., accelerometer, gyroscope, and magnetometer), and more computation overhead. At the high packet rate scenarios, ATPS gets enough feedback to learn the channel dynamic and properly schedule the transmissions. Hence, it outperforms both Chimp and Tuatara.

The number of transmissions in DPPI is between 16% to 27% more than that of ATPS. It consumes more energy and potentially produces more interference. FLP performs the worst, dropping up to 66% of the packets. Compared to ATPS it consumes between 20% to 130% more energy.

In a low packet rate scenario, ExPerio cannot detect the periodicity in the channel pattern and sends all packets using power level 7, similar to FHP. Hence, they both achieve the lowest number of transmissions, however, at the expense of the highest potential interference. At a high packet rate, ExPerio detects the periodicity after a while, thus, it schedules the packets to be transmitted using power level 1 at the channel peaks through which it saves energy slightly more than ATPS. However, detecting the channel periodicity and its peaks requires a lot of transmissions with the maximum power level and imposes an unaffordable computation overhead [9].

In summary, ATPS learns channel state transition probabilities through channel monitoring and feedback analysis. Unlike ExPerio, which has high computation overhead and is designed for periodic body postures, ATPS supports both static and dynamic postures without significant computation and memory burdens. Moreover, ATPS outperforms Tuatara and Chimp in high packet rate scenarios for dynamic postures.

VII. Conclusion

This paper presents IGE, a memory-efficient Markov chain that accurately predicts the channel behavior in WBANs. Motivated by the high accuracy of IGE for long-term channel prediction, ATPS, an adaptive transmission power selection scheme for reliable, low-energy, and low-interference communication in WBANs is developed. ATPS enables the sending node to benefit from the channel prediction model for scheduling packet transmissions. ATPS monitors the channel fluctuations and learns the channel pattern. Then, it buffers the packets when the channel is bad and schedules them to be transmitted when the channel is expected to become good within a deadline. The experimental results in many scenarios demonstrate that this scheme can self-adapt to changes in channel fluctuation patterns and choose the most appropriate power level to reduce energy consumption and interference and improve communication reliability when the packet rate is high. ATPS decreases the usage of high transmission signal power and accordingly reduces energy usage significantly, without any remarkable packet loss overhead.

References

[1] LAN/MAN-Standards-Committee, "802.15.4 - IEEE standard for local and metropolitan area networks–part 15.4: Low-rate wireless personal area networks (lr-wpans)," *IEEE std*, p. 314, 2011.

[2] LAN/MAN-Standards-IEEE-Committee, "802.15.6 - IEEE standard for local and metropolitan area networks - part 15.6: Wireless body area networks," *IEEE std*, p. 271, 2012.

[3] W.-S. Baek, D.-M. Kim, F. Bashir, and J.-Y. Pyun, "Real life applicable fall detection system based on wireless body area network," in *IEEE Consumer Communications and Networking Conference (CCNC)*, 2013, pp. 62–67.

[4] J. C. Chan, H. Leung, J. K. Tang, and T. Komura, "A virtual reality dance training system using motion capture technology," *IEEE Transactions on Learning Technologies*, vol. 4, no. 2, pp. 187–195, 2011.

[5] B. Zhou, H. Koerger, M. Wirth, C. Zwick, C. Martindale, H. Cruz, B. Eskofier, and P. Lukowicz, "Smart soccer shoe: monitoring football interaction with shoe integrated textile pressure sensor matrix," in *Proceedings of the 2016 ACM International Symposium on Wearable Computers*. ACM, 2016, pp. 64–71.

[6] G. Grimm, G. Guilmin, F. Poppen, M. S. Vlaming, and V. Hohmann, "The personal hearing system–a software hearing aid for a personal communication system," *EURASIP Journal on Advances in Signal Processing*, vol. 2009, no. 1, pp. 1–9, 2009.

[7] G. Li, B.-L. Lee, and W.-Y. Chung, "Smartwatch-based wearable eeg system for driver drowsiness detection," *IEEE Sensors Journal*, vol. 15, no. 12, pp. 7169–7180, 2015.

[8] K. Y. Yazdandoost and K. Sayrafian-Pour, "Tg6 channel model id: Ieee 802.15-08-0780-12-0006," *IEEE 802.15 working group document*, 2009.

[9] A. Arghavani, H. Zhang, Z. Huang, and Y. Chen, "Chimp: A learning-based power-aware communication protocol for wireless body area networks," *ACM Transactions on Embedded Computing Systems (TECS)*, vol. 18, no. 2, p. 18, 2019.

[10] Texas-Instruments, "CC2420 datasheet," *http://www.ti.com/lit/ds/symlink/cc2420.pdf*, 2007.

[11] UC. Berkeley, "TelosB datasheet," *http://www2.ece.ohio-state.edu/~bibyk/ee582/telosMote.pdf*, 2004.

[12] D. Smith, J. Zhang, L. Hanlen, D. Miniutti, D. Rodda, and B. Gilbert, "Temporal correlation of dynamic on-body area radio channel," *Electronics Letters*, vol. 45, no. 24, pp. 1212–1213, 2009.

[13] L. Xiao, S. Hong, S. Xu, H. Yang, and X. Ji, "Irs-aided energy-efficient secure wban transmission based on deep reinforcement learning," *IEEE Transactions on Communications*, vol. 70, no. 6, pp. 4162–4174, 2022.

[14] K. S. Kumar and B. Sujatha, "Fpga design of an efficient eeg signal transmission through 5g wireless network using optimized pilot based channel estimation: a telemedicine application," *Wireless Personal Communications*, vol. 123, no. 4, pp. 3597–3621, 2022.

[15] L. Tong and Q. Zhao, "Joint order detection and blind channel estimation by least squares smoothing," *IEEE Transactions on Signal Processing*, vol. 47, no. 9, pp. 2345–2355, 1999.

[16] J.-C. Lin, "Least-squares channel estimation for mobile ofdm communication on time-varying frequency-selective fading channels," *IEEE Transactions on Vehicular Technology*, vol. 57, no. 6, pp. 3538–3550, 2008.

[17] D. B. Smith, T. Lamahewa, L. W. Hanlen, and D. Miniutti, "Simple prediction-based power control for the on-body area communications channel," in *Communications (ICC), 2011 IEEE International Conference on*. IEEE, 2011, pp. 1–5.

[18] M. Quwaider, J. Rao, and S. Biswas, "Transmission power assignment with postural position inference for on-body wireless communication links," *ACM Transactions on Embedded Computing Systems (TECS)*, vol. 10, no. 14, p. 27, 2010.

[19] S. Kim, S. Kim, and D.-S. Eom, "Rssi/lqi-based transmission power control for body area networks in healthcare environment," *IEEE Journal of Biomedical and Health Informatics*, vol. 17, no. 3, pp. 561–571, 2013.

[20] L. Hanlen, V. Chaganti, B. Gilbert, D. Rodda, T. Lamahewa, and D. Smith, "Open-source testbed for body area networks: 200 sample/sec, 12 hrs continuous measurement," in *Personal, Indoor and Mobile Radio Communications Workshops (PIMRC Workshops), 2010 IEEE 21st International Symposium on*. IEEE, 2010, pp. 66–71.

[21] J. Zhang, D. Smith, and Z. Chen, "Linear finite state markov chain predictor for channel prediction," in *Personal Indoor and Mobile Radio Communications (PIMRC), 2012 IEEE 23rd International Symposium on*. IEEE, 2012, pp. 2085–2089.

[22] E. N. Gilbert, "Capacity of a burst-noise channel," *Bell system technical journal*, vol. 39, no. 5, pp. 1253–1265, 1960.

[23] E. O. Elliott, "Estimates of error rates for codes on burst-noise channels," *Bell system technical journal*, vol. 42, no. 5, pp. 1977–1997, 1963.

[24] B. Liu, Z. Yan, and C. W. Chen, "Medium access control for wireless body area networks with qos provisioning and energy efficient design," *IEEE Transactions on Mobile Computing*, vol. 16, no. 2, pp. 422–434, 2017.

[25] H. A. Sanneck and G. Carle, "Framework model for packet loss metrics based on loss runlengths," in *Electronic Imaging*. International Society for Optics and Photonics, 1999, pp. 177–187.

[26] P. Kindt, H. Jing, N. Peters, and S. Chakraborty, "Experio-exploiting periodicity for opportunistic energy-efficient data transmission," in *IEEE Conference on Computer Communications (INFOCOM)*, 2015, pp. 82–90.

[27] A. Arghavani, H. Zhang, and Z. Huang, "LPA: Learning-based power aware communication protocol in WBANs," in *IEEE Conference on Pervasive Intelligence and Computing (PICom)*, 2016, pp. 512–519.

[28] W. Zang and Y. Li, "Gait cycle driven transmission power control scheme for wireless body area network," *IEEE Journal of Biomedical and Health Informatics*, vol. 22, no. 3, pp. 697–706, 2017.

[29] ——, "Motion aware transmission power control scheme in wireless body area network," in *Signal Processing Systems (SiPS), 2015 IEEE Workshop on*. IEEE, 2015, pp. 1–5.

[30] A. Arghavani, H. Zhang, Z. Huang, Y. Chen, and Z. Chen, "Tuatara: Location-driven power-adaptive communication for wireless body area networks," *IEEE Transactions on Mobile Computing*, 2021.

[31] B. Liang, X. Liu, H. Zhou, V. C. Leung, A. Liu, and K. Chi, "Channel resource scheduling for stringent demand of emergency data transmission in wbans," *IEEE Transactions on Wireless Communications*, vol. 20, no. 4, pp. 2341–2352, 2020.

[32] P. Soldati, H. Zhang, and M. Johansson, "Deadline-constrained transmission scheduling and data evacuation in wirelesshart networks," in *2009 European Control Conference (ECC)*. IEEE, 2009, pp. 4320–4325.

[33] Z. Zou, P. Soldati, H. Zhang, and M. Johansson, "Energy-efficient deadline-constrained maximum reliability forwarding in lossy networks," *IEEE Transactions on Wireless Communications*, vol. 11, no. 10, pp. 3474–3483, 2012.

[34] Y. Li, H. Zhang, Z. Huang, and M. Albert, "Optimal link scheduling for delay-constrained periodic traffic over unreliable wireless links," in *IEEE INFOCOM 2014-IEEE Conference on Computer Communications*. IEEE, 2014, pp. 1465–1473.

[35] Z. Yang, Z. Zhou, and Y. Liu, "From rssi to csi: Indoor localization via channel response," *ACM Computing Surveys (CSUR)*, vol. 46, no. 2, pp. 1–32, 2013.
[36] R. L. Blessey, H. J. Hislop, R. L. Waters, and D. Antonelli, "Metabolic energy cost of unrestrained walking," *Physical therapy*, vol. 56, no. 9, pp. 1019–1024, 1976.
[37] A. Arghavani, H. Zhang, Z. Huang, and Y. Chen, "Atps: Adaptive transmission power selection for communication in wireless body area networks," in *2017 IEEE 42nd Conference on Local Computer Networks (LCN)*. IEEE, 2017, pp. 615–618.
[38] Y. Rafiq, "Online markov chain learning for quality of service engineering in adaptive computer systems," Ph.D. dissertation, University of York, 2015.

Abbas Arghavani earned his Ph.D. in Computer Science from the University of Otago, New Zealand, in 2019. Following his Ph.D., he joined Uppsala University, Sweden, as a Postdoctoral Fellow, a position he held until 2022. Currently, he is an Associated Senior Lecturer at Mälardalen University, Sweden. Abbas's research spans a range of topics in wireless communications, the Internet of Things, Machine Learning, and Game Theory. He has actively participated in organizing several international conferences, serving as a program chair or co-chair. He is also a valued member of the program committee board for various international conferences.

Haibo Zhang received the MSc. degree in Computer Science from Shandong Normal University, China, in 2005 and the Ph.D. degree in Computer Science from the University of Adelaide, Australia, in 2009. From 2009 to 2010, he was a Postdoctoral Researcher with the Automatic Control Laboratory at the Royal Institute of Technology (KTH), Stockholm, Sweden. He is currently an Associate Professor with the Department of Computer Science, University of Otago, New Zealand. His research interests include wireless sensor networks, 5G networks, vehicular ad-hoc networks, routing protocol design/analysis, and machine learning. He has published over 100 peer-reviewed papers in conference proceedings and international journals. He has served as program chair or co-chair for more than 15 international conferences and has been on the program committee board for many international conferences.

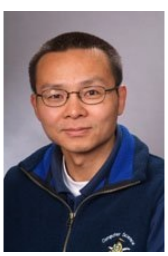

Zhiyi Huang received the BSc degree in 1986 and the PhD degree in 1992 in computer science from the National University of Defense Technology (NUDT) in China. He is a Professor at the Department of Computer Science, University of Otago, New Zealand. He was a visiting professor at EPFL (Swiss Federal Institute of Technology Lausanne) and Tsinghua University in 2005, and a visiting scientist at MIT CSAIL in 2009. His research fields include parallel/distributed computing, parallel machine learning algorithms, multicore architectures, operating systems, green computing, cluster/grid/cloud computing, high-performance computing, signal processing, and computer architectures. He has published over 150 papers in well-known conferences and journals.

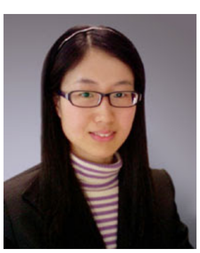

Yawen Chen is a Senior Lecturer at the Department of Computer Science, University of Otago, New Zealand. She obtained her PhD degree in Computer Science from the University of Adelaide in Australia in 2008. Her research interests include resource optimization and performance evaluation in computer networking and computer architecture (optical network-on-chips, interconnection network, wired and wireless networking).